Chapter 4

Application of Graphene Gas Sensors in Online Monitoring of SF_6 Insulated Equipment

Xiaoxing Zhang, Ju Tang, Song Xiao and Cheng Pan

Additional information is available at the end of the chapter

http://dx.doi.org/10.5772/intechopen.68329

Abstract

Graphene is an allotrope of carbon apart from graphite, diamond, fullerene and carbon nanotubes. Because graphene has unique mechanical, structural, thermal and electrochemical properties and can present the stability characteristics of these features, it becomes two-dimensional (2-d) materials which can alter three-dimensional (3-d) carbon nanotubes composite materials and has important research value. Pristine graphene and graphene films doped with Au nanoparticles were synthesized by the chemical reduction method. Their corresponding gas sensors were both fabricated by the traditional drop coating method and then used as an adsorbent for the detection of H_2S, SO_2, SOF_2 and SO_2F_2 at room temperature. Theoretical simulation was also investigated when the decomposed gaseous components of sulfur hexafluoride (SF_6), namely, H_2S, SO_2, SOF_2 and SO_2F_2, were adsorbed on pristine and Au-embedded graphene based on DFT. In order to interpret the adsorption processes between Au-doped graphene and gas molecules, this chapter discussed the charge transfer mechanism on the adsorption surface for further investigation.

Keywords: graphene, properties, preparation methods, characterization analysis, Au-decorated graphene, experimental response

1. Introduction of graphene

1.1. Properties of graphene

Graphene is an allotrope of carbon apart from graphite, diamond, fullerene and carbon nanotubes, and it is also a kind of atomic crystal with two-dimensional laminar nano-structure materials. It was first prepared by Professor Geim in the University of Manchester by the micro-mechanical

stripping method [1]. The discovery of the new material confirmed that a strict two-dimensional material existed in the nature. The research group of Professor Geim found that the new materials had unique, excellent physical and chemical properties and had great development potential and application space in super capacitor, biochemical, fuel cell, etc. after carrying out system characterization on electrical properties of graphene. Professor Geim and Dr Novoselov won the Nobel Prize for physics in 2010 for a groundbreaking research. This raised a hot wave of graphene research.

The thickness of the monolayer graphene is only 0.34 nm, that is, the thickness of the layer of carbon atoms [2]. The outer electron distribution of C-atoms is $2s^2 2p^2$, two 2s electrons and one 2p electron form two-dimensional hexagonal honeycomb structure by sp^2 hybridization. **Figure 1** is the diagram of graphene configuration and **Figure 2** is the band structure of graphene. The strong C-C bonds making the graphene layer has excellent structural rigidity. Each carbon atom

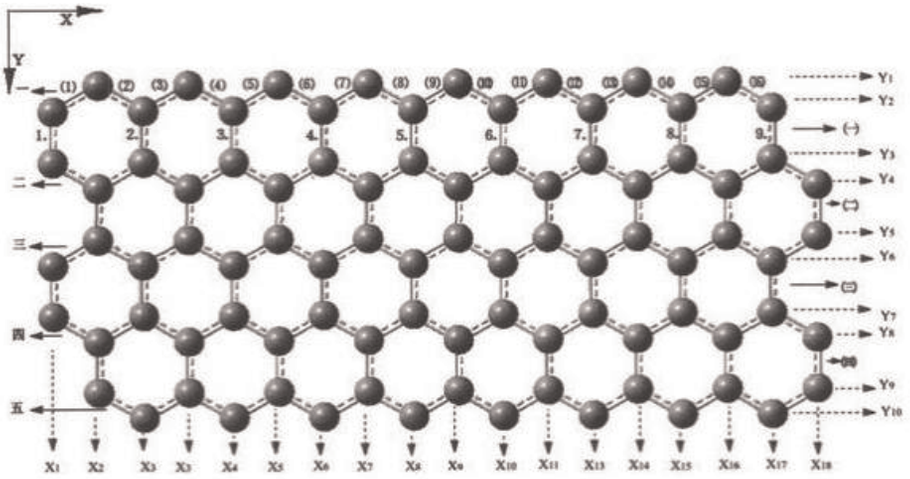

Figure 1. Graphene configuration diagram.

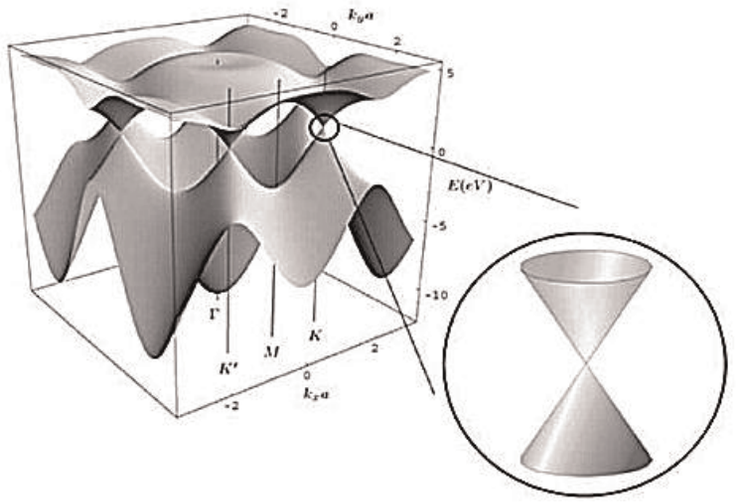

Figure 2. Graphene band structure.

has a non-binding 2p free electron. These electrons process free motion in delocalized π-orbitals which were formed in the vertical direction of carbon atoms plane. Thus, graphene has good electrical conductivity [3]. By analyzing the energy band structure of graphene and brillouin zone map, we can find that the conduction band and valence band are like cone-shaped valleys [4, 5]. They are highly symmetrical in the brillouin zone and form a double cone. There is a linear relationship between amplitude of the momentum and the change of the energy. The conduction band and valence band just intersect at six points of Fermi level. The state density is 0 at these six points. Because of the unique structure of graphene [4], it has incomparable excellent properties compared with other materials. At present, the physical properties which have been confirmed include:

- The carrier concentration of graphene is $10^{12}/cm^2$ and the electrical resistivity is 10^{-6} Ω/cm^3. It has been found that graphene is the best conductor at room temperature [6].
- Single layer graphene has ultra-high carrier mobility at room temperature, which can reach 2×10^5 cm^2/Vs [7].
- Each carbon atom can act as the surface atom on graphene, as all carbon atoms are exposed. Therefore, graphene has a large specific surface area, which has a theoretical value of 2630 m^2/g [8].
- Graphene has extremely low Johnson noise under the condition of small carries amount. Therefore, a very small change of carrier concentration will cause significant change in the conductivity [9].
- The typical electronic conduction velocity of graphene is 8×10^5 m/s, nearly 1/400 of the propagation velocity of light in vacuum and much larger than electrical conduction rate of general semiconductor materials [10].

1.2. Preparation methods of graphene

Because graphene has unique mechanical, structural, thermal and electrochemical properties and can present the stability characteristics of these features, it becomes 2-d materials which can alter 3-d carbon nanotubes composite materials and has important research value. These superior properties, however, depend largely on the process of separating graphite substrate into the nano-sized level of the graphene layer. As carbon nanotubes and other nano-composite materials, the first problem before graphene materials that can be widely used is how to synthesis single layer or fewer layers of high-quality graphene. How to get complete structure and disperse graphene evenly in a solution becomes the second biggest problem among scholars around the world. In addition, due to the interaction of van der Waals force, graphene may irreversibly stack and accumulate unless graphene layers completely separate. But the majority of superior physical and chemical properties of graphene materials only exists in single-layer graphene. Therefore, the synthesis of graphene has a vital influence in its application in various fields. Effectively preventing it from stacking and accumulating is particularly important. If one summarizes achievements in the field of graphene synthesis in recent years, scholars mainly found the exfoliation method, several synthetic methods, etc. Different synthetic methods can be chosen according to different applications:

1.2.1. Mechanical exfoliation method

The mechanical exfoliation method is the simplest way of preparation of graphene [11, 12]. Research group of Geim first got single-layer graphene by this method [8]. This was only a 0.34 nm of two-dimensional layered nanostructures atomic crystal. The significance of this study was that it confirmed that the perfect two-dimensional crystal can also stably exist in finite temperature and corrected the fallacy that a two-dimensional crystal cannot exist in finite temperature stability in material science field. This method uses high orientation pyrolysis graphite (HOPG) as raw materials, and the specific steps are: make HOPG of 1 mm deep from a square platform of 5-μm deep after oxygen plasma etching and adhere the square platform on the photoresist and extrude properly. Repeatedly strip off the graphene sheets from square HOPG piece using transparent tape. At last, dissolve the graphene which adheres on the photoresist in acetone and transfer it to the silicon substrate and process ultrasonic treatment. Remove the thicker sheet and get the graphene of less than 10 nm thick. It is generally believed that this type of method for preparing graphene layers can get single layer and fewer layers of graphene which have relatively good crystal structure, least structure defects and excellent physical and chemical properties. But this method is time consuming and cannot effectively control the thickness of graphene layer. It is also vulnerable to tape pollution and the yield is very low. So, this method cannot realize large-scale preparation of graphene synthesis.

In general, the mechanical exfoliation method is still the most effective method for preparation of single layer or fewer layer of high-quality graphene. This method is suitable for the laboratory basic theory research.

1.2.2. Chemical stripping method

Chemical stripping method is the method that by using oxidizing graphite, remove the oxygen-containing functional groups between the graphite layers so as to get a large area of graphene [12, 13]. At present, there are mainly three methods (Brodie, Staudenmaier and Hummers) for graphite oxidation treatment. Among them, Hummers is most commonly used because preparation process parameters can be easily modified and effectively reduce emissions of poison. After oxidation treatment, the flake graphite layers interact mainly by weak van der Waals force, effectively improving the graphite layer spacing. Removing oxygen-containing functional groups between graphite layers includes both chemical reduction and thermal reduction method. The main reducers used in chemical reduction method are hydrazine, vitamin C, etc. Hydrazine is a kind of strong polarity toxic compounds. Research has confirmed that environmental vitamin C can also obtain good reduction effect. No matter what kind of reducing agent is chosen, chemical reduction process will inevitably leave a certain amount of oxygen, resulting in lower conductivity of graphene by the chemical reduction method compared with the mechanical stripping method. Heat treatment is also an effective method for reducing oxidized graphite, which works effectively in alkaline environment or in microwave conditions. At present, there is research that combined the chemical reduction and thermal reduction methods to reduce oxidized graphite. Overall, chemical stripping method is an effective method to realize the large-scale preparation of graphene, which has the advantages of fewer layers, high yield, and is easy to operate, but the graphene

prepared by the method is easily polluted by the addition of dispersion solvent; the crystal structure has some defects and is somewhat mixed and disorderly. Therefore, this method is suitable for sensor and catalytic applications where the conductivity requirements are not rigorous.

1.2.3. Chemical vapor deposition (CVD) method

Chemical vapor deposition method is the most accepted method for preparation of large size monolayer or fewer layers of high-quality graphene [14–16]. Graphene is the first compound prepared by Somani research team using this method. In CVD method, graphene growth needs the high temperature of around 1000°C and must have a fast cooling process. Hydrocarbon gases such as methane, methanol act as carbon source, interact with foil catalytic media like nickel, drill or copper. Under the suitable growth temperature, the carbon element inside the gas will effectively dissolve in metal foil, similar to the carburizing process. Then, in the rapid quenching process, the carbon dissolved in the metal foil separate out of the surface, thus forming a layer of uniform, a relatively perfect and large size of crystal structure of graphene films. From growth mechanism, the thickness and crystalline sequence of the graphene by this method are decided mainly by the quenching rate, thickness of metal foil and the carbon content dissolved in the metal foil. Graphene prepared by the CVD method can be easily transferred to other basement, such as SiC, SiO_2 substrate, and can also be cut to suitable size according to its uses which provides convenience for the subsequent application. In any case, the CVD method provides graphene synthesis method for a layer of controllable size, regular crystal of monolayer or fewer layers of high-quality graphene, which makes it possible to have large production of thin film electrode in volume. The disadvantages of this method include complexity of process and relatively high cost.

1.2.4. Epitaxial method

Ultrahigh vacuum thermal treatment of SiC is an effective way to obtain high-quality graphene layers [17, 18], especially in semiconductor manufacturing industry. The graphene prepared by this method is widely used because it is directly used with insulating properties of SiC for substrate without any complex substrate transfer process which can be directly assembled. When 6H-SiC single crystal in ultra-high vacuum conditions is heated to a certain temperature, Si atoms on the surface will sublimate from the basal surface because of its higher vapor pressure, and the C atom not sublimated will stay on the basal surface rearranged to form honeycomb stable structure, which becomes the graphene layer. The thickness of the graphene layers depends on the annealing time and heating temperature. The study shows that the condition for the preparation of fewer layers of graphene is treated with the high temperature of 1200–1600°C after 1 hour, and then have a few minutes of SiC annealing treatment. According to a study, the high temperature of 1600°C on SiC substrate is more advantageous to form a uniform fewer layer graphene. Despite the epitaxial method, it is worth looking forward to, but there are a few questions that need to be resolved. First of all, how to precisely control the thickness of the large size graphene film in the actual production is the first challenge to face. Second, epitaxial graphene layers grown on different surfaces in SiC (Si, C surface) differ in structure, thickness, even some physical properties and electrical properties,

and the mechanism of above differences has not obtained any breakthrough. The relationship of structure and electron properties between two layers, between lamella and substrate, is the third challenge for further study. Anyhow, graphene prepared by epitaxial method only bases on SiC and cannot be transferred to other substrate, which limits its application in other areas.

1.2.5. Other synthetic methods

In addition to several commonly used preparation methods introduced above, there are other methods like organic synthesis method, cracking carbon nanotube method, arc discharge method [19]. Organic synthesis is mainly used to form graphene-like hydrocarbons polymer (PAHs) by organic reactions. Although this method can realize diversity of synthesis, grafting boundary, changing solubility and many other advantages, the biggest question is how to stably store, spread and form a large area of two-dimensional plane PAHs. Cracking the carbon nanotube method mainly depends on carbon nanotubes, these contain curling graphene layers. The advantage of this method is that the preparation methods of different size carbon nanotubes have ease of application, so the size of the graphene layer can be controlled effectively by etching and cracking of hydrogen plasma. For amorphous carbon, the arc discharge method is used to obtain perfect lattice and stable graphene by high temperature plasma modification of amorphous carbon and H: etching. Studies have demonstrated that the arc discharge process is actually a fast thermal reduction process, which prepares high conductivity and stable graphene after liquid phase separation and centrifugation.

2. Decorated graphene

2.1. Gas sensing properties of pristine graphene and Au-decorated graphene to SOF_2, SO_2F_2, SO_2 and H_2S through simulation

We investigated the adsorption effects of gaseous molecules on pristine graphene and Au-graphene. **Figure 3(a)–(h)** shows the most stable adsorption configurations of H_2S, SO_2, SO_2F_2 and SOF_2 on pristine graphene and Au-graphene. All presented stable configurations have the lowest energies of various adsorption sites with different gas molecular orientations. We focused on the adsorption of H_2S, SO_2, SOF_2 and SO_2F_2 [20].

2.1.1. H_2S adsorption

We mainly considered eight possible configurations for an H_2S molecule on pristine graphene: four different orientations for H atoms close to the C plane, three different configurations for S atoms close to the C plane and a configuration for an H_2S molecule parallel with the C plane. Comparing these binding energies, two H atoms perpendicular to the graphene surface on the hollow site, shown in **Figure 3(a)**, is the most thermodynamically stable configuration. **Table 1** details the calculated results for adsorption distance, E_{ad}, bond length, charge transfer (CT) and magnetic moment for the entire system of H_2S adsorbed on pristine graphene and Au-graphene. The results show that the geometric structure of H_2S (1.356 Å for H-S bond length and 91.076 for H-S-H bond angle) practically remains the same as in the gas phase. The

http://dx.doi.org/10.5772/intechopen.68329

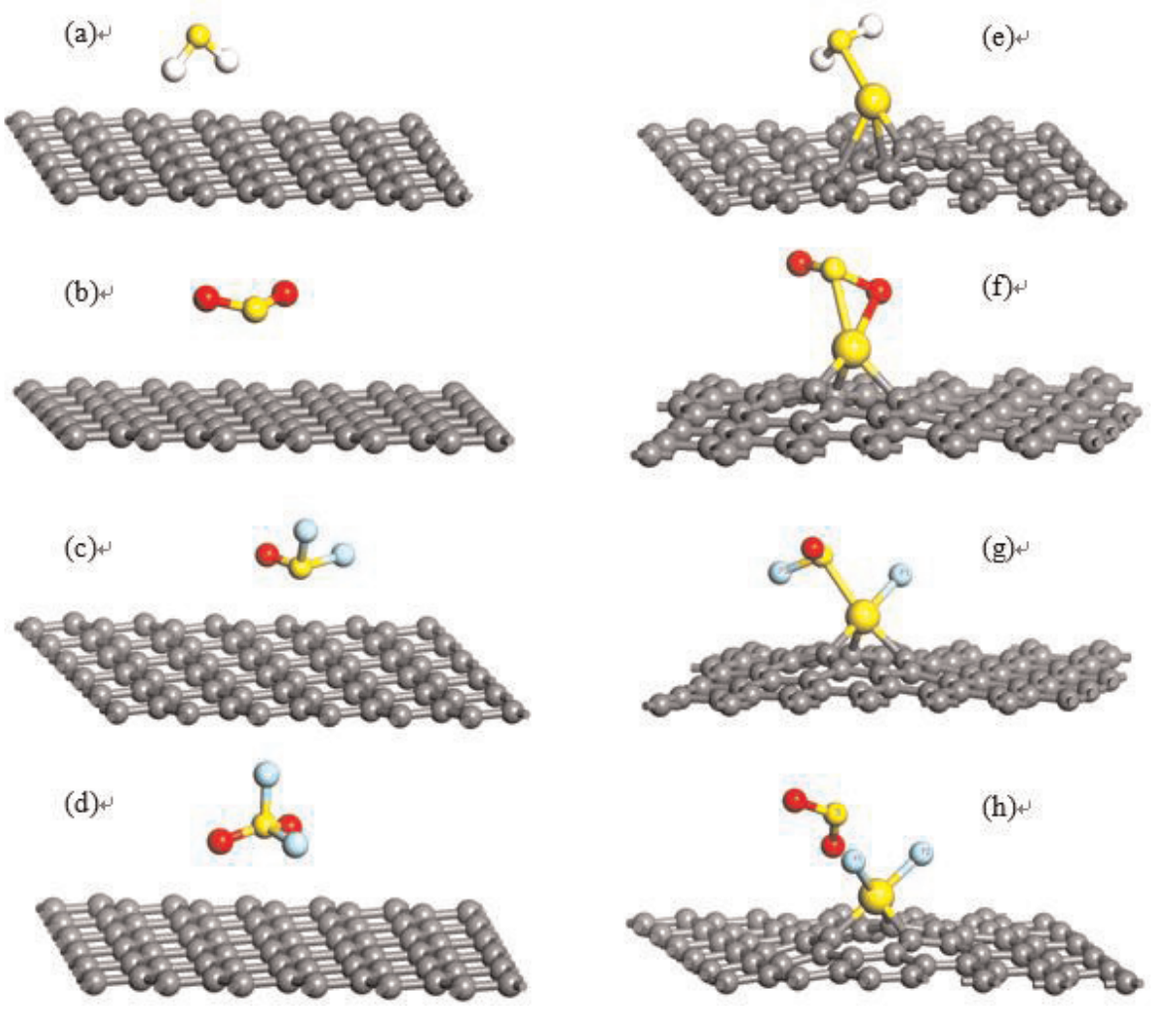

Figure 3. (a)–(d) Optimized configurations for H_2S, SO_2, SOF_2 and SO_2F_2 adsorbed on pristine graphene; (e)–(h) optimized configurations for H_2S, SO_2, SOF_2 and SO_2F_2 adsorbed on Au-graphene. Various configurations were considered; only the most stable ones were presented.

Configuration	d (Å)	E_{ad} (eV)	Bond length (Å)	Q_t (e)	M (μ_B)
Au-graphene	\	\	\	\	−1.005
H_2S	\	\	1.356 (S-H)	\	0
H_2S on graphene	3.108	−0. 717	1.356 (S-H)	+0.011	0
H_2S on Au-graphene	2.401	−0.900	1.360 (S-H_1), 1.362 (S-H_2)	+0.348	0.999

Table 1. H_2S adsorption on pristine graphene and Au-graphene: adsorption distance (d), adsorption energy (E_{ad}), bond length, charge transfer from H_2S to the substrate (Q_t), and magnetic moment of the entire system (M).

Mulliken population analysis demonstrates that fewer than 0.011 electrons are transferred from the H_2S molecule to the pristine graphene. The E_{ad} (−0.717 eV) is a relatively strong intermediate between physisorption and chemisorption, which indicates that van der Waals acts as a main factor.

Figure 3(e) shows that H_2S is adsorbed parallel to the graphene surface with the S atom closest to the Au-graphene plane in all original positions of Au-graphene. The geometric structure of H_2S changed only slightly; the H-S-H bond angle became 91.719, while each H-S bond length became 1.360 and 1.362 Å, respectively. However, adsorption distance decreased to 2.401 Å, and E_{ad} significantly increased to 0.90 eV. A total of 0.348 electrons got transferred from the H_2S molecule to Au-graphene, which leads to electron enrichment of the Au-graphene surface. These results reveal a stronger interaction in the Au-graphene adsorption system than in the pristine one.

The calculated density of states (DOS) for pristine graphene and Au-graphene, with and without a single H_2S molecule, are plotted in **Figure 4(a)** to further understand H_2S interaction with the Au-graphene surface. A slight difference was observed near the Fermi level, which indicates a decrease in the surrounding DOS and a magnetism alteration of the magnetic moment to 0.999 μ_B is obtained. **Figure 4(b)** shows an analysis of partial DOS (PDOS) for the H_2S molecule and Au atom. **Table 2** lists orbital CTs. The 3p of S in H_2S and 5-d orbital of Au are hybridized between −9 and −1.1 eV in a valence band with a certain filling rate degree in PDOS peaks. A comparison between **Figure 4(b)** and **Table 2** shows that the electrons in the 5-d orbital of Au that are populated to initially empty spin-down π^* are obtained, which leads to a strong interaction between Au and H_2S.

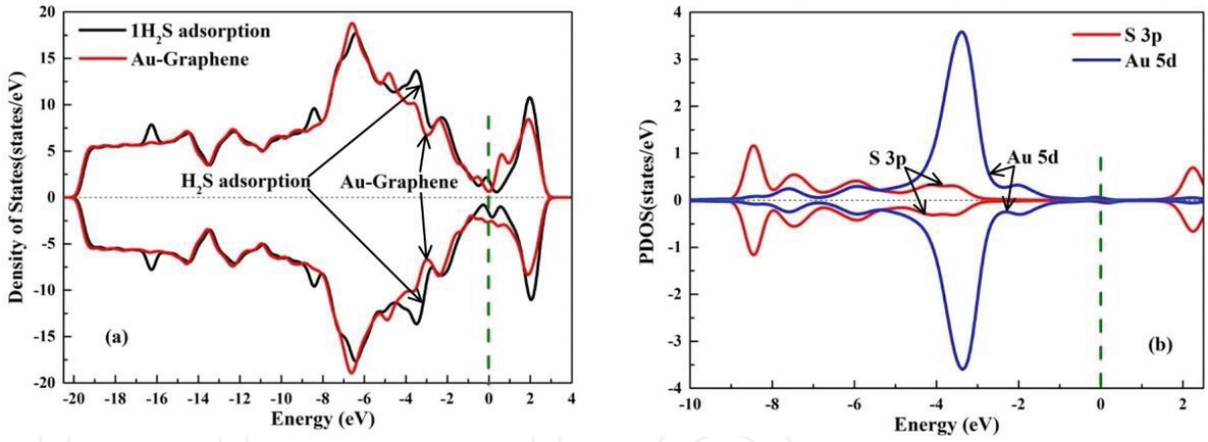

Figure 4. (a) Spin-polarized total DOS for Au-graphene with and without single H_2S adsorption; (b) PDOS projected on the 3p of S in H_2S and 5d orbital of Au. Fermi energy is set to $E-E_f$.

Element	s (e)	p (e)	d (e)	Charge (e)	Spin (μ_B)
Au	−0.28	−0.336	+0.432	−0.184	0.049
S	+0.237	−0.178	−0.202	−0.141	−0.005
H_1	+0.272	−0.03	\	0.241	0.000
H_2	+0.279	−0.03	\	0.248	0.001

Table 2. H_2S adsorption on Au-graphene: charges transfer in s, p and d orbitals, and total charge, spin magnetic moment of a single atom.

2.1.2. SO_2 adsorption

Figure 3(b) shows that the most energetically favorable configuration for SO_2 adsorption on pristine graphene is the S atom on top of the T site carbon atom, with SO_2 lying nearly parallel to the surface and the S atom, tilting slightly toward it. Three configurations for the S atom initially approached the graphene plane because of the different orientations on the carbon ring. These configurations include three positions for two O atoms close to it and one configuration for the SO_2 molecule parallel to it; they are all studied. The calculated E_{ad} and d are 0.302 eV and 3.335 Å, respectively. S-O bond length and bond angle are at 1.482 Å and 119.550, respectively; they remain almost the same as in the gas phase (1.480 Å and 119.916). A total of 0.012 electrons transfer from the pristine graphene to the SO_2 molecule. Consequently, SO_2 undergoes van der Waals interaction on pristine graphene.

Figure 3(f) shows that SO_2 is adsorbed with one S-O bond approaching Au in the Au-graphene substrate; a significant increase in E_{ad} and CT and a notable decrease in adsorption distance are observed. **Table 3** details all these values. The close S-O bond is expanded from 1.480 Å in the gas phase to 1.609 Å in the adsorption system, with the bond angle (O-S-O) changing from 119.550 to 114.944. This stable configuration exhibits a 0.351 eV charge flow from Au-graphene to the SO_2 molecule, which indicates that SO_2 has a charge acceptor nature. These findings indicate that a stronger interaction occurred on Au-graphene (−0.587 eV) compared with pristine graphene (−0.302 eV). However, chemisorption with a binding energy above 0.8 eV was not observed.

Figure 5(a) shows the DOS for Au-graphene with and without single SO_2 molecule adsorption. The PDOS for Au and SO_2 were also plotted in **Figure 5(b)**. Asymmetrical spin-up and spin-down channels maintain metallicity. The spin-up channel of SO_2 adsorption on Au-graphene is obviously altered near the Fermi level, which leads to a magnetic moment of 0.948 μ_B for the entire system. The 5-d electrons of Au are hybridized with π states of S and O at −6.5eV in the valence band, which is indicated in the atomic population analysis results (**Table 4**). This hybridization results in a strong E_{ad} to SO_2.

2.1.3. SOF_2 adsorption

Adsorption of an uncommon SOF_2 is more complicated than that of H_2S or SO_2. SOF_2 and SO_2F_2 adsorption on graphene-based materials has not been studied. We thoroughly investigate two kinds of gases. For SOF_2 on pristine graphene, we considered the S atom down to the graphene surface with three positions (H, T and B sites) and the F and O parallel atoms down to the plane with two different orientations. **Figure 3(c)** shows that the configuration of

Configuration	d (Å)	E_{ad} (eV)	Bond length (Å)	Q_t (e)	M (μ_B)
SO_2	\	\	1.480 (S-O)	\	0
SO_2 on graphene	3.335	−0.302	1.482 (S-O)	−0.012	0
SO_2 on Au-graphene	2.176	−0.587	1.609 (O_1-S), 1.501 (O_2-S)	−0.351	0.948

Table 3. SO_2 adsorption on pristine graphene and Au graphene: adsorption distance (d), adsorption energy (E_{ad}), bond length, charge transfer from the substrate to SO_2 (Q_t), and magnetic moment of the entire system (M).

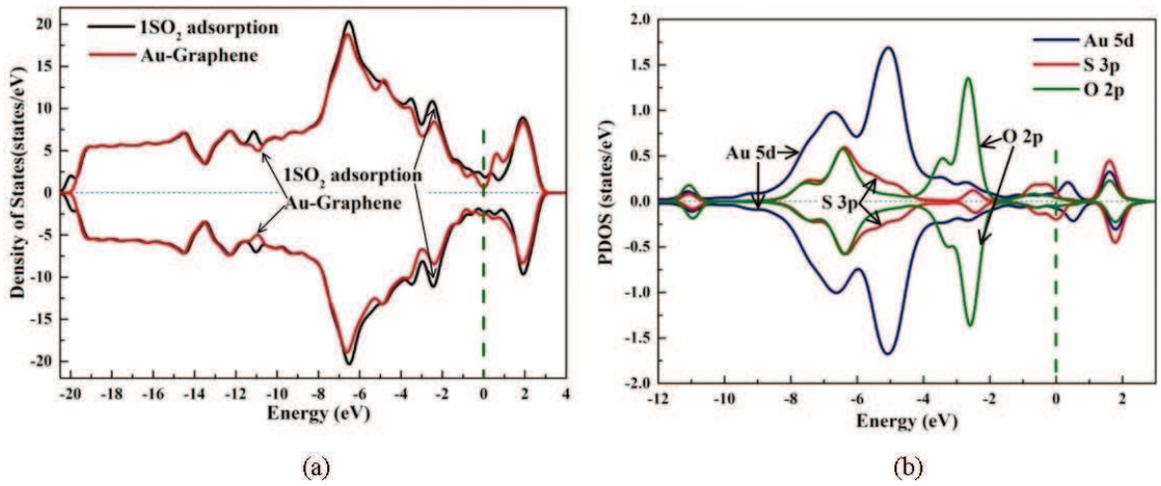

Figure 5. (a) Spin-polarized total DOS for Au-graphene with and without single SO_2 adsorption; (b) PDOS projected on the 3p of S, 2p of O in SO_2 and 5d orbital of Au. Fermi energy is set to E-E_f.

Element	s (e)	p (e)	d (e)	Charge (e)	Spin (μ_B)
Au	−0.057	−0.763	+0.794	−0.023	0.044
S	+0.217	+0.908	−0.776	0.350	0.107
O_1	+0.119	−0.481	−0.037	−0.397	0.022
O_2	+0.163	−0.427	−0.038	−0.304	0.111

Table 4. SO_2 adsorption on Au-graphene: charge transfer in s, p and d orbitals, and total charge spin magnetic moment of a single atom.

S close to the graphene plane top on the bridge (B) site, is the most stable one according to the calculated adsorption energies, with E_{ad} of −0.467 eV. **Table 5** details the adsorption parameters. The Mulliken population analysis indicates that 0.002 electrons shifted from graphene to SOF_2, which is not considered an apparent interaction with the pristine surface, and the charges shift value is meaningless for chemical interaction. SOF_2 bond lengths and bond angles substantially remain the same. Therefore, the electron interaction between SOF_2 and the pristine surface is negligible, and the van der Waals interaction plays a significant role in this case.

Configuration	*d* (Å)	E_{ad} (eV)	Bond length (Å)	Q_t (e)	*M* (μ_B)
SOF_2	\	\	1.459 (S-O), 1.668 (S-F)	\	0
SOF_2 on graphene	3.526	−0.467	1.461 Å (S-O), 1.670 Å (S-F)	−0.002	0
SOF_2 on Au-graphene	2.039	−0.961	2.894 (S-F_1), 1.72 (S-F_2)		
1.501 (O-S)	−0.624	0			

Table 5. SOF_2 adsorption on pristine graphene and Au-graphene: adsorption distance (*d*), adsorption energy (E_{ad}), bond length, charge transfer from the substrate to SOF_2 (Q_t), and magnetic moment of the entire system (*M*).

http://dx.doi.org/10.5772/intechopen.68329

The situation was different for Au-graphene. **Figure 3(g)** shows that SOF_2 preferred the configuration with the S atom on top of the H site and the S-F bond extended to 2.894 Å, which is likely to rupture. One F atom is possibly bonded to Au, which is indicated by the distance between F and Au (2.039 Å). The preferred adsorption configuration is a stable geometric configuration where the electron-rich F and Au interact. A similar situation occurred between the Au and S. **Table 5** shows a large electron transfer and SOF_2 exhibits a charge acceptor-like feature.

Figure 6(a) shows that the DOS for Au-graphene with a single SOF_2 molecule significantly changed near the Fermi level unlike with H_2S and SO_2. The spin-up and spin-down channels are shifted toward a high-energy direction. The SOF_2 adsorption turns magnetic Au-graphene into a non-magnetic system. However, this phenomenon has not been observed in the H_2S and SO_2 adsorption systems. Combining **Figure 6(b)** and **Table 6**, the electrons in the π states of F are transferred from the 5-d orbital of metal Au on adsorption. The electrons are strongly hybridized at −2.25 eV in the valence band. The occupied 3p orbital of S is broadened and shifted far below the Fermi level, which is hybridized with the 5-d orbital of Au. The original empty d orbital of S also participates in hybridization, which

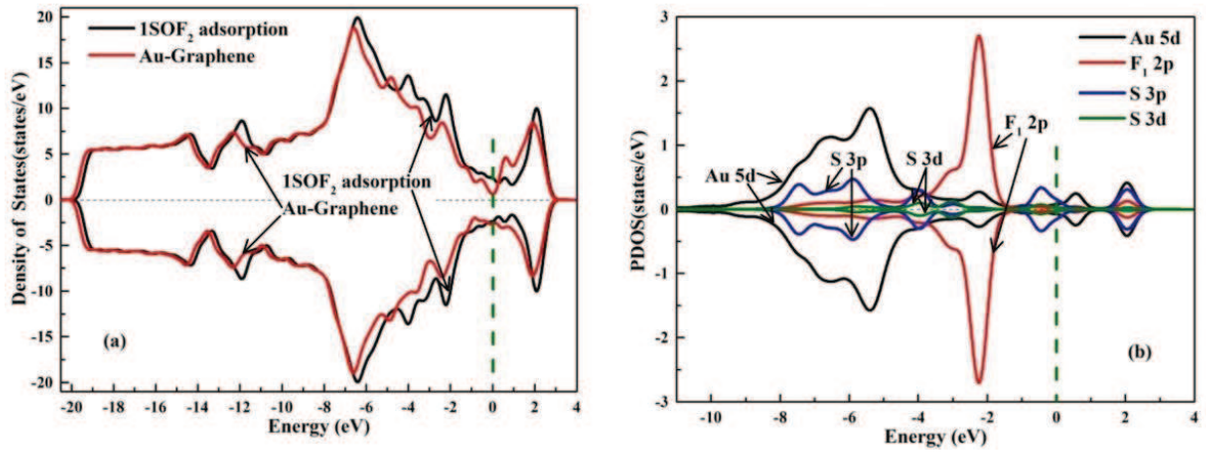

Figure 6. (a) Spin-polarized total DOS for Au-graphene with and without single SOF_2 adsorption; (b) PDOS projected on 3p and 3d of S, 2p orbital of F1 in SOF_2 and 5d orbital of Au. Fermi energy is set to $E\text{-}E_f$.

Element	s (e)	p (e)	d (e)	Charge (e)	Spin (μ_B)
Au	−0.032	−0.852	+0.898	0.014	0.000
S	+0.22	+0.914	−0.636	0.500	0.000
O	+0.164	−0.424	−0.04	−0.300	0.000
F_1	+0.032	−0.530	−0.01	−0.508	0.000
F_2	+0.044	−0.342	−0.016	−0.317	0.000

Table 6. SOF_2 adsorption on Au-graphene: charges transfer in s, p and d orbitals, and total charge spin magnetic moment of a single atom.

leads to accumulation of electrons. These findings suggest the strong influence of Au-graphene on the chemical reactivity of SOF_2 adsorption.

2.1.4. SO_2F_2 adsorption

Figure 3(d) and **(h)** reveal the lowest-energy configurations for SO_2F_2 adsorption on pristine graphene and Au-graphene, respectively. Only six original configurations were considered on the pristine graphene because of the highly symmetrical structure of SO_2F_2. These configurations include one orientation with two F atoms and one O atom close to the graphene substrate and another orientation with two O atoms and one F atom close to the plane. The two orientations must consider the relative locations on the plane (H, B and T sites). The most stable configuration is ultimately with two F, one S and two O atoms directly on every close-in C atom, which leaves the S atom on top of the T site carbon. The geometry of SO_2F_2 remains unchanged, which indicates rare interaction on the pristine one. This finding is consistent with the generally accepted idea that pristine graphene has weak interaction with common small gaseous molecules (excluding NO_2 and NH_3) because of its dangling bond shortage [21, 22].

A strong interaction is observed on Au-graphene. **Table 7** details the adsorption parameters. SO_2F_2 is adsorbed with the two F atoms bonded to Au in the substrate, while the bond lengths of S-F significantly increased. SO_2F_2 has a good chance of dissociating into SO_2 because electron-rich F atoms play a vital role in the adsorption process. The SO_2F_2 molecule pulls electrons away from Au-graphene. Unlike cases for H_2S, SO_2 and SOF_2 adsorbates, a significantly large electron shift occurs in SO_2F_2 due to adsorption on Au-graphene. This electron shift affects the local distribution of the adsorption system and significantly changes electron properties.

Therefore, we observe the DOS for Au-graphene with SO_2F_2 molecule adsorption. **Figure 7(a)** shows that magnetism disappears because of SO_2F_2; a similar case for SOF_2 is observed. SO_2F_2 causes a finite DOS within a band at a certain degree below Fermi level. A significant conductance change is expected because of the notable DOS change obtained from the Fermi level, which is highly consistent with the electron shift analysis. **Figure 7(b)** and **Table 8** show a strong interaction between Au and F atoms that occurred with an orbital mixing according to calculated PDOS and the atomic population analysis results for each atom, respectively. The accumulated electrons that occupied the π orbital of the two F atoms are mainly derived from

Configuration	d (Å)	E_{ad} (eV)	Bond length (Å)	Q_t (e)	M (μ_B)
SO_2F_2	\	\	1.609 Å (S-F), 1.441 Å (S-O)	\	0
SO_2F_2 on graphene	3.472	−0.472	1.609 (S-F_2), 1.610 (S-F_2)	−0.004	0
			1.442 (O_2-S), 1.441 (O_1-S)		
SO_2F_2 on Au-graphene	2.035	−1.790	3.145 (S-F_2), 2.095 (S-F_2)	−0.967	0
			1.477 (O_2-S), 1.545 (O_1-S)		

Table 7. SO_2F_2 adsorption on pristine graphene and Au-graphene: adsorption distance (d), adsorption energy (E_{ad}), bond length, charge transfer from the substrate to SO_2F_2 (Q_t), and magnetic moment of the entire system (M).

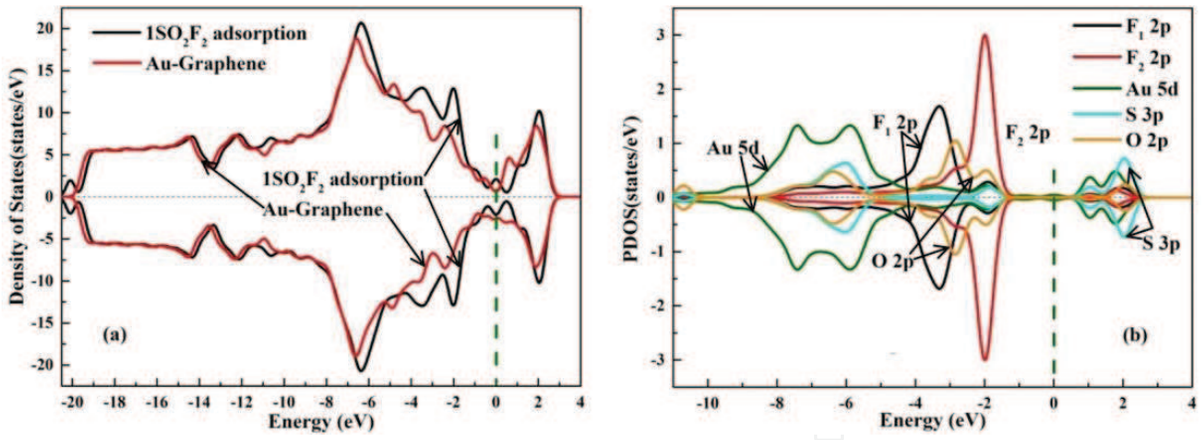

Figure 7. (a) Spin-polarized total DOS for Au-graphene with and without single SO_2F_2 adsorption; (b) PDOS projected on the 3p of S, 2p of O, 2p orbital of F1 and F2 in SO_2F_2 and 5d orbital of Au. Fermi energy is set to E-E_f.

Element	s (e)	p (e)	d (e)	Charge (e)	Spin (μ_B)
Au	+0.05	−0.876	+1.023	0.197	0.000
S	+0.204	+1.21	−0.836	0.577	0.000
O_1	+0.172	−0.388	−0.04	−0.256	0.000
O_2	+0.156	−0.488	−0.036	−0.367	0.000
F_1	+0.032	−0.532	−0.012	−0.506	0.000
F_2	+0.034	−0.438	−0.01	−0.415	0.000

Table 8. SO_2F_2 adsorption on Au-graphene: charges transfer in s, p and d orbitals, and total charge spin magnetic moment of a single atom.

the 5-d orbital of Au. They appear with a certain hybridization degree in the valence band not far from the Fermi level. This condition provides a valuable reason for S-F bond breakage and formation of Au-F bonds.

2.2. Preparation methods of Au-decorated graphene

Au-decorated Graphene films (GrF) was synthesized through the following chemical reduction procedure [23]: carboxyl functionalized graphene (1 mg) was dispersed in 5 mL $HAuCl_4$ (1 mM) solution as precursor under constant sonication for 40 min to reach a stable colloid state; 5 mL $NaBH_4$ (40 mM) solution was added dropwise to the above colloid mixed solution with vigorous stirring for 30 min; centrifugal separation step was then followed; the resulting products were collected and washed with distilled water for several times; and were finally dried in a vacuum oven at 60°C for 12 h to obtain the Au-doped GrF. Au-doped GrF powders (5 mg) were dispersed ultrasonically in 200 mL DMF solution for 30 min to reach a relatively good dispersibility.

Then, we describe the methods of sensors fabrication and sensing performance. The sensors based on Au-doped GrF were fabricated by layer-by-layer (LBL) deposition method [24]. Then, the responses were measured by monitoring surface resistance change in a pressure-tight system. As to the planar sensor, depicted in **Figure 8**, copper electrodes were interdigitally etched on epoxy resin with approximately 30-μm foil thickness and 0.2-mm electrode gap. Quantitative prepared and dispersed Au-doped GrF solution was continuously dropped on the substrate with accompanied drying treatment to the substrate until the initial surface resistance values met the needs. In short, uniform, dense and smooth deposited films were the destination [25]. Thus, an expected Au-doped GrF sensor was ready for detection. Then, the sensing element was placed in the autonomous sealed chamber and connected to an electrochemical analyzer. Here, it is worth noting that initial vacuum resistance stability is a prerequisite for the following gas detection. Response measurements were all carried out at room temperature and repeated several times to obtain reliable results.

2.3. Characterization analysis of Au-decorated graphene

Analyses of material are basically required. Preliminary, **Figure 9(a)** exhibits X-ray diffraction (XRD) patterns of the Au-doped GrF and reduced graphene oxide (rGO). The Au characteristic peaks in Au-doped GrF are observed at 38.1 (111), 44.3 (200), 64.5 (220), 77.55 (311) and 81.65 (222), as compared with the standard Au peaks at 38.184 (111), 44.392 (200), 64.576 (220), 77.547 (311) and 81.721 (222), respectively. The main Au (111) peak suggests the crystal phase formed and the broad Au peaks imply that highly dispersed Au nanoparticals (AuNPs) exist in the sample [20]. Particle size estimated from the main peak width of Au (111) suggests 14 nm according to the Scherer formula. Meanwhile, broad diffraction peaks at 24.63 and 23.77 for Au-doped GrF and rGO samples exhibit the carbon structure of graphene.

Then, Raman spectra were introduced for structural characterization [26]. Typical post-subtraction Raman spectra recorded directly on the sensor substrate are exhibited in **Figure 9**. Note that, for the epoxy layers underlying the films are insulating, the effect on the electron distribution is not considered here. A comparison of the Raman spectra between Au-doped GrF and pure rGO films concludes that the presence of low amount doped AuNPs does not seriously change the formation of in-plane sp^2 domains of graphene. The Raman spectra for the films indicate representative peaks at 1358/cm (D), 1591/cm (G) along with broad bands

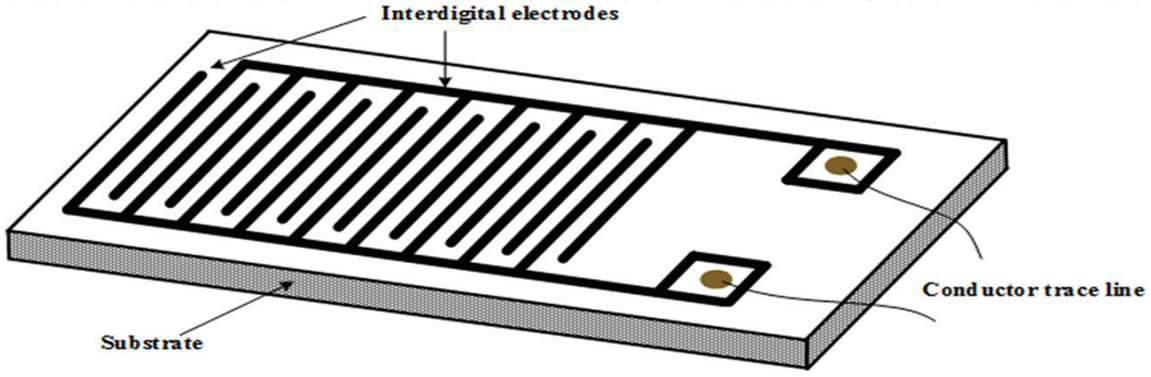

Figure 8. Schematic structural view of the planar sensor.

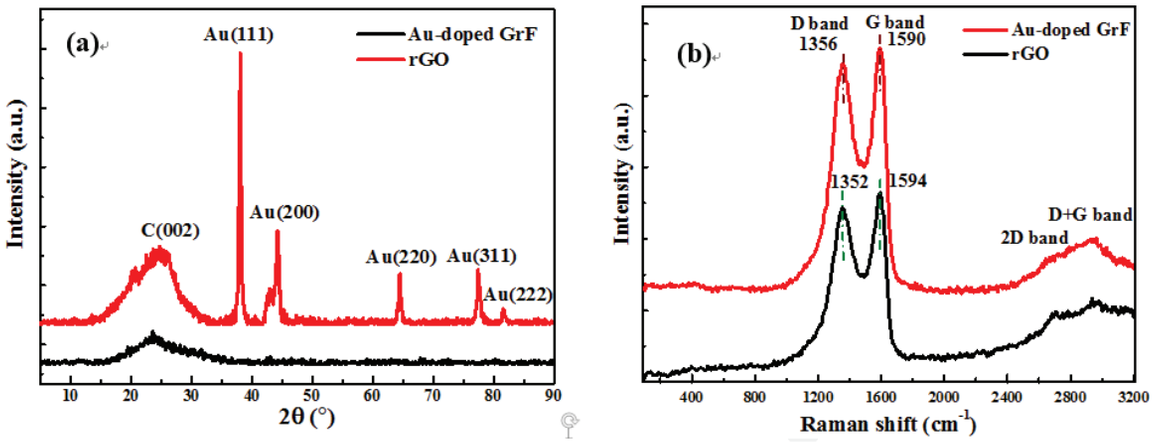

Figure 9. (a) XRD patterns of rGO and Au-doped GrF; (b) Raman spectra of rGO and Au-doped GrF.

between 2400/cm and 3200/cm. The ratio of intensities of the D and G peaks is highly sensitive to the quality of material [27], from which we speculate that the graphene-based materials are multilayers. Furthermore, the D-peak is quite obvious, indicative of a significant number of defects and a degree of confusion structure, which is caused by deprivation of parts of oxygen functionalities during the hydrogen reduction [28]. A size of tens to hundreds nanometers are concluded for these sample flakes according to the D/G ratio of 0.85 and the G peak position. This observation is roughly in accordance with the XRD analysis.

The morphological structure, particle size and metal dispersion of Au-doped GrF films are examined by SEM, as shown in **Figure 10(b)**. The enhanced area caused by the highly dispersed AuNPs enables more available active sites on the sensing surface. From these results, AuNPs are uniformly embedded in and covered on the rGO. After analyzing numerous images, the average diameter of AuNPs is tens of nanometers, in agreement with the XRD and Raman studies [20]. The TEM morphologies of Au-doped GrF are shown in **Figure 10(c)–(d)**. The TEM images also prove that AuNPs with dozens of nanometers sizes are homogenously dispersed on rGO sheets surface. A close observation of high-resolution TEM images in **Figure 3(d)** inset indicates well-defined lattice fringes of Au (111) with the clear lattice distance ($d_{111} = 0.235$ nm), showing that the AuNPs exist and are highly crystalline. Moreover, the EDS spectrum verifies again the Au element successfully doped in graphene.

As is well known, XPS spectra play a significant role in valence analysis. The XPS signatures of rGO and Au-doped GrF are shown in **Figure 11**. In accordance with XRD, SEM and TEM, the XPS results reveal that approximately 6% AuNPs have successfully doped on the graphene surface. The high-resolution C 1s XPS spectrum of rGO indicates a plenty of heteroatom defects existing on the plane and edges, in which the C 1s spectrum can be fitted into four peaks, corresponding to C atom in four different kinds of functional groups: the nonoxygenated ring C at 284.8 eV, the C in C-N bond at 285.8 eV, the hydroxyl C at 286.8 eV and the carbonyl C at 288.6 eV. After Au was introduced, the new peak at 284.2 eV appears, which is attributed to the C-N-Au bond [29]. After peak-differentiation-imitating, Au 4f doublet deconvolutes into two pair of peaks, corresponding to the reduced Au (0) at 84.27 eV in Au $4f_{7/2}$ and 87.94 eV in Au $4f_{5/2}$; the Au (III) ions at 85.02 eV in Au $4f_{7/2}$ and the Au (I) ions at

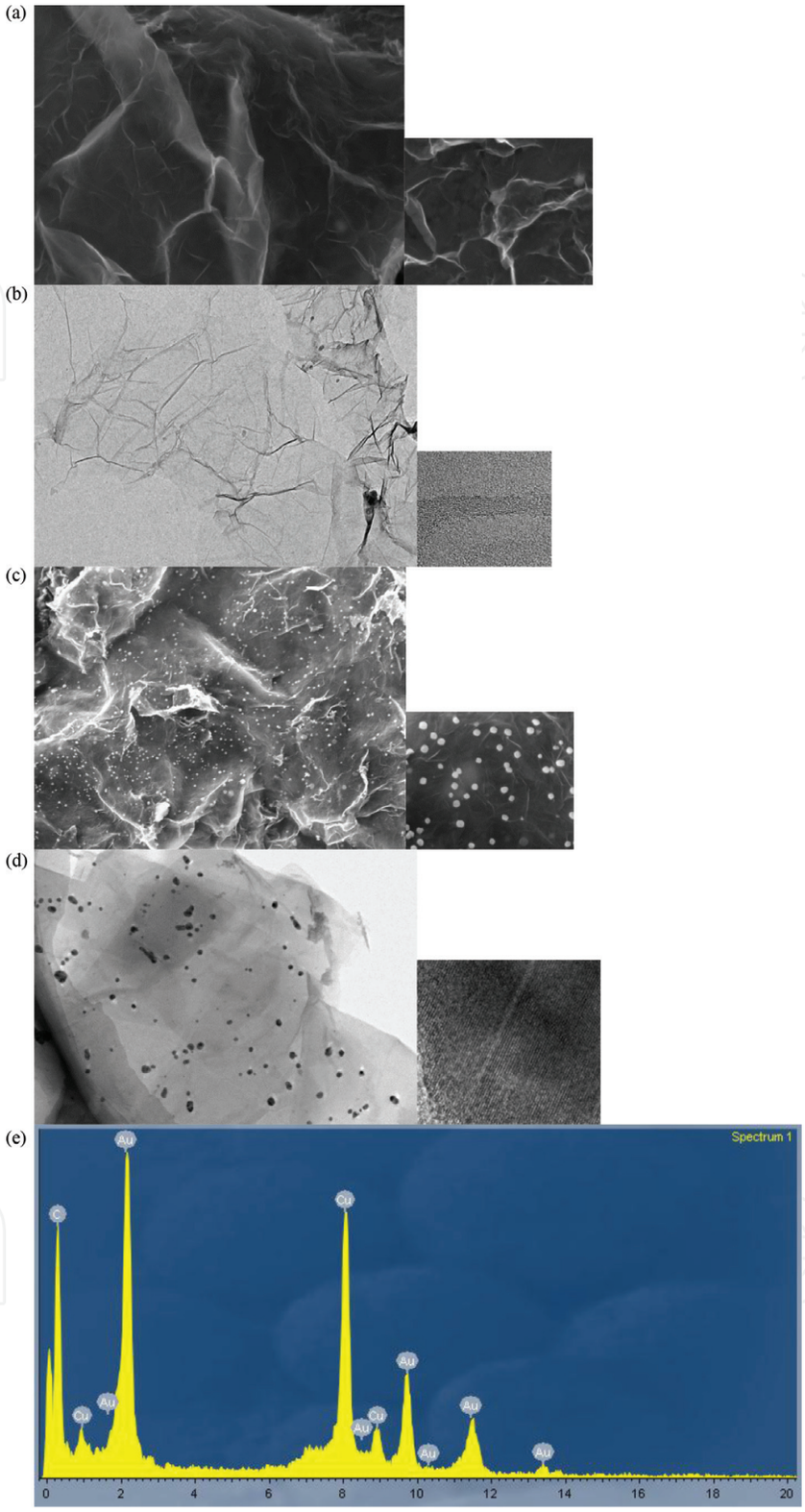

Element	Weight%	Atomic%
C K	27.31	76.09
Cu K	32.41	17.07
Au M	40.28	6.84

Figure 10. (a) rGO SEM image; (b) Au-doped GrF SEM image; (c) rGO TEM and HRTEM image inset; (d) Au-doped GrF TEM and HRTEM image inset; (e) EDS spectrum of Au-doped GrF.

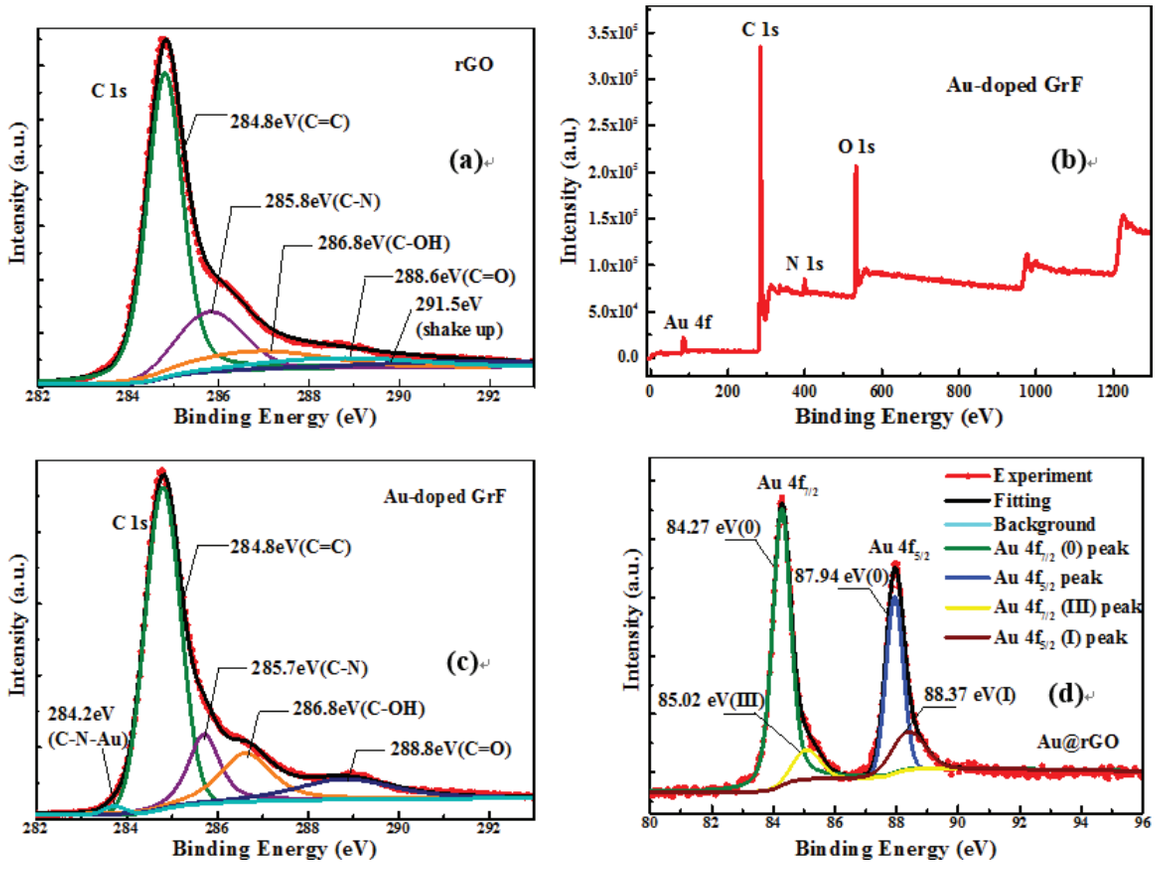

Figure 11. XPS spectra of the (a) C 1s region of rGO; (b) survey spectrum of Au-doped GrF; (c) C 1s region of Au-doped GrF; and (d) Au 4f region of Au-doped GrF.

88.37 eV in Au $4f_{5/2}$, respectively. Compared with the XPS of bulk Au (83.7 eV), there exists a nearly 0.6 eV red shift of XPS peak of Au (0) ions in Au $4f_{7/2}$. Such shift in the bonding energy may be ascribed to the underlying substrate and the reduced core-hole screening in metal particles. Furthermore, a dynamic electron transfer from the doped AuNPs to the support graphene films is proved by the existence of positively charged Au (III) and Au (I) ions according to the electrostatic balance principle [20], which is also confirmed by the following theoretical calculation in our density functional theory (DFT) study.

2.4. Experimental response of Au-decorated graphene

Figure 12(a)–(b) gives the rGO and Au-doped GrF sensor responses in terms of change in resistance obtained during the varied concentrations of target gases exposure in the autonomous sealed chamber. The change of resistance is defined as

$$\Delta R = R_F - R_I \tag{1}$$

where R_F represents the sensor resistance at the final target gas exposure and R_I represents the initial vacuum resistance at the previous rest period. Here, the sensor response is universally defined as [30]:

$$\text{Sensitivity} = \frac{\Delta R}{R_I} \times 100\% \tag{2}$$

Though humidity and temperature have a significant effect on the sensor response, the specific operating conditions in electrical equipment will reduce this variation. **Figure 12(a)–(d)** shows the sensor responses after exposure to 50 and 100 ppm of H_2S and SOF_2, respectively. For the purpose of exploring the sensing mechanism, here we only present the responses at this two-concentration atmosphere. In ambient conditions, for rGO, 100 ppm H_2S causes 15.78% reduction in resistance as much as 10.53% for lower concentration of 50 ppm. And then, SOF_2 is found to be insensitive to rGO. As illustrated in **Figure 5(d)**, 100 ppm SOF_2 results in 23.83% reduction to Au-doped GrF and the change is 15.36% for 50 ppm SOF_2, which indicates a larger sensitivity of Au-doped GrF to SOF_2 in comparison to rGO. Also, Au-doped GrF is tested to be sensitive to H_2S, but the opposite resistance change is observed. Note that 100 ppm H_2S increases the resistance by 28.15% and 50 ppm makes 18.73% addition. The sensing performance of Au-doped GrF and bare rGO may be of value in selective detection application. Therefore, the sensing behaviors are required to be analyzed in much more detail [20, 31].

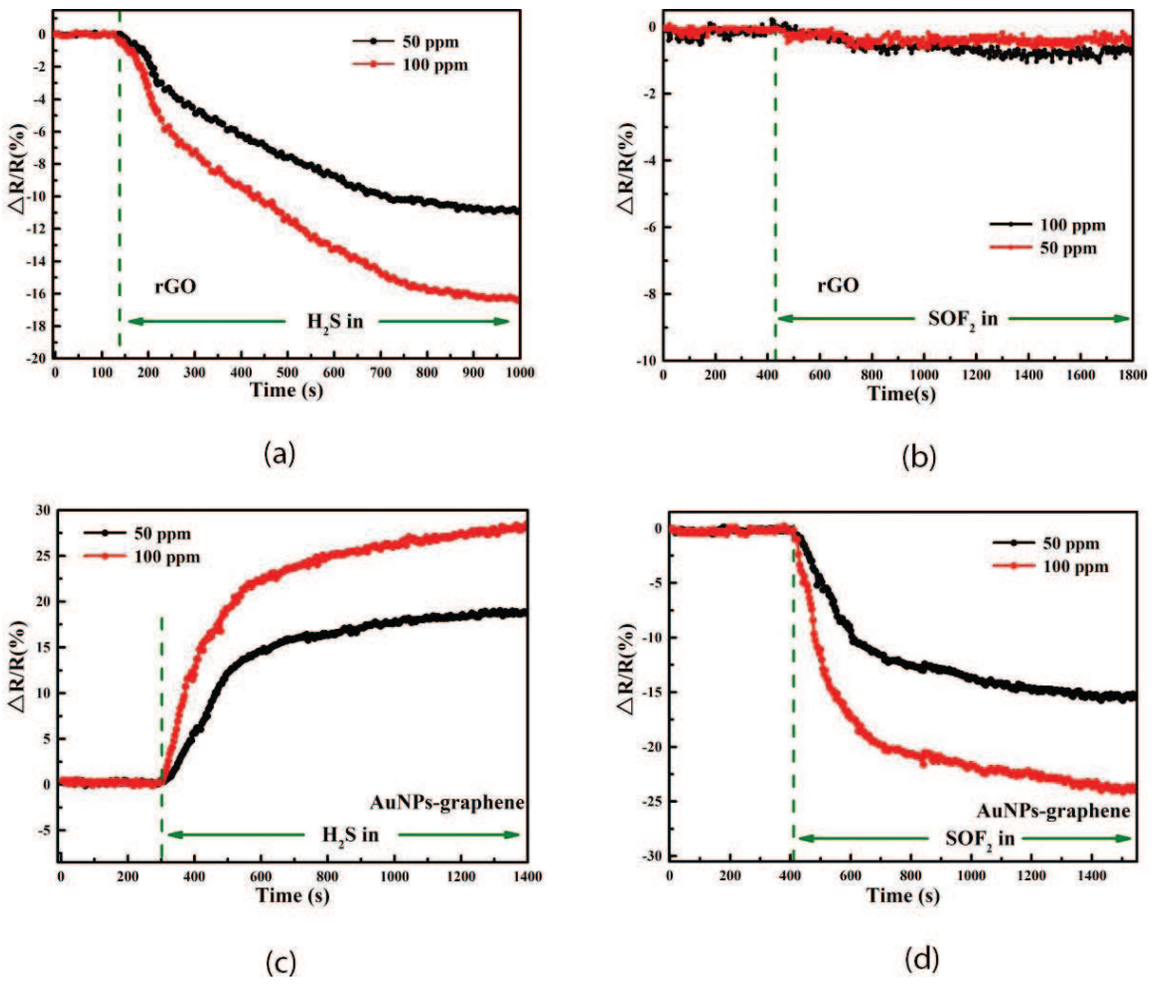

Figure 12. Experimental response transients of rGO sensors to (a) H_2S, (b) SOF_2; Au-doped GrF sensors to (c) H_2S, (d) SOF_2.

Acknowledgements

Parts of this chapter are reproduced from Ref. [31] with Elsevier's permission.

Author details

Xiaoxing Zhang*, Ju Tang, Song Xiao and Cheng Pan

*Address all correspondence to: xiaoxing.zhang@outlook.com

School of Electrical Engineering, Wuhan University, Wuhan, China

References

[1] Novoselov KS, Geim AK, Morozov SV, et al. Electric field effect in atomically thin carbonfilms. Science. 2004;**306**(5696):666–669

[2] Lee C, Wei X, Kysar JW, et al. Measurement of the elastic properties and intrinsic strength of monolayer graphene. Science. 2008;**321**(5887):385–388

[3] Neto AHC, Guinea F, Peres NMR, et al. The electronic properties of graphene. Reviews of Modern Physics. 2009;**81**(1):109

[4] Geim AK. Graphene: Status and prospects. Science. 2009;**324**(5934):1530–1534

[5] Wakabayashi K. Graphene and its Fascinating Attributes. World Scientific Publishing Company; 2011

[6] Dragoman M, Dragoman D. Graphene-based quantum electronics. Progress in Quantum Electronics. 2009;**33**(6):165–214

[7] Verma R, Bhattacharya S, Mahapatra S. Modeling of temperature and field-dependent electron mobility in a single-layer graphene sheet. IEEE Transactions on Electron Devices. 2013;**60**(8):2695–2698

[8] Wang C, Li Z, Guo Z, et al. A novel hydrazine electrochemical sensor based on the high specific surface area graphene. Microchimica Acta. 2010;**169**(1):1–6

[9] Karasik BS, Mckitterick CB, Prober DE. Prospective performance of graphene HEB for ultrasensitive detection of sub-mm radiation. Journal of Low Temperature Physics. 2014;**176**(3–4):249–254

[10] Ptitsin VE. Electron beam ablation phenomenon--theoretical model and applications. Applied Optics. 1987;**26**(19):4036–4038

[11] Lotya M, Hernandez Y, King PJ, et al. Liquid phase production of graphene by exfoliationof graphite in surfactant/water solutions. Journal of the American Chemical Society. 2009;**131**(10):3611–3620

[12] Stankovich S, Dikin DA, Piner RD, et al. Synthesis of graphene-based nanosheets via chemical reduction of exfoliated graphite oxide. Carbon. 2007;**45**(7):1558–1565

[13] Eda G, Fanchini G, Chhowalla M. Large-area ultrathin films of reduced graphene oxide as a transparent and flexible electronic material. Nature Nanotechnology. 2008;**3**(5):270–274

[14] Bhaviripudi S, Jia X, Dresselhaus MS, et al. Role of kinetic factors in chemical vapor deposition synthesis of uniform large area graphene using copper catalyst. Nano Letters. 2010;**10**(10):4128–4133

[15] Li X, Cai W, An J, et al. Large-area synthesis of high-quality and uniform graphene films on copper foils. Science. 2009;**324**(5932):1312–1314

[16] Chae SJ, Günes F, Kim KK, et al. Synthesis of large-area graphene layers on poly-nickel substrate by chemical vapor deposition: wrinkle formation. Advanced Materials. 2009;**21**(22):2328–2333

[17] Forbeaux I, Themlin JM, Debever JM. Heteroepitaxial graphite on 6H-SiC (0001): Interface formation through conduction-band electronic structure. Physical Review B. 1998;**7658**(24):16396

[18] Emtsev KV, Bostwick A, Horn K, et al. Towards wafer-size graphene layers by atmospheric pressure graphitization of silicon carbide. Nature Materials. 2009;**8**(3):203–207

[19] Singh V, Joung D, Zhai L, et al. Graphene based materials: past, present and future. Progress in Materials Science. 2011;**56**(8):1178–1271

[20] Zhang X, Yu L, Wu X, Hu W. Experimental sensing and density functional theory study of H_2S and SOF_2 adsorption on Au-doped graphene. Advanced Science. 2015;**2**(11):612–612

[21] Ran Q, Gao M, Guan X, Wang Y, Yu Z. First-principles investigation on bonding formation and electronic structure of metal-graphene contacts. Applied Physics Letters. 2009;**94**:103511

[22] Geng W, Liu H, Yao X. Enhanced photocatalytic properties of titania-graphene nanocomposites: A density functional theory study. Physical Chemistry Chemical Physics. 2013;**15**:6025–6033

[23] Hu Y, Xue Z, He H, Ai R, Liu X, Lu X. Photoelectrochemical sensing for hydroquinone based on porphyrin-functionalized Au nanoparticles on graphene. Biosensors & Bioelectronics. 2013;**47**:45–49

[24] Qureshi SS, Zheng Z, Sarwar MI, Félix O, Decher G. Nanoprotective Layer-by-Layer coatings with epoxy components for enhancing abrasion resistance: Toward robust multimaterial nanoscale films. ACS Nano. 2013;7:9336–9344

[25] Lei Y, Zhang X, Tang J. The sensitive characteristics study of SF_6, decomposed gases using a graphene sensor. In: International Conference on High Voltage Engineering and Application (ICHVE); IEEE; 2014. 1–4

[26] Wang G, Yang J, Park J, Gou X, Wang B, Liu H, Yao J. Facile synthesis and characterization of graphene nanosheets. Journal of Physical Chemistry C. 2008;**112**:8192–8195

[27] Cançado LG, Jorio A, Martins Ferreira EH, et al. Quantifying defects in graphene via Raman spectroscopy at different excitation energies. Nano Letters. 2011;**11**(8):3190–3196

[28] Li Y, Yu Y, Wang JG, Song J, Li Q, Dong M, Liu CJ. CO oxidation over graphene supported palladium catalyst. Applied Catalysis B: Environmental. 2012;**125**:189–196

[29] Yin H, Tang H, Wang D, Gao Y, Tang Z. Facile synthesis of surfactant-free Au cluster/graphene hybrids for high-performance oxygen reduction reaction. Acs Nano. 2012;**6**:8288–8297

[30] Bai S, Guo T, Zhao Y, Sun J, Li D, Chen A, Liu CC. Sensing performance and mechanism of Fe-doped ZnO microflowers. Applied Catalysis B: Environmental. 2014;**195**:657–666

[31] Zhang X, Yu L, Gui Y, et al. First-principles study of SF_6 decomposed gas adsorbed on Au-decorated graphene. Applied Surface Science. 2016;**367**:259–269

IntechOpen